

Nickel–aluminum layered double hydroxides prepared via inverse micelles formation

María E. Pérez-Bernal, Ricardo J. Ruano-Casero, Fátima Benito, Vicente Rives*

GIR-QUESCAT, Departamento de Química Inorgánica, Universidad de Salamanca, 37008 Salamanca, Spain

ARTICLE INFO

Article history:

Received 4 November 2008

Received in revised form

3 March 2009

Accepted 7 March 2009

Available online 20 March 2009

Keywords:

Layered double hydroxides

Mixed oxides

Chromatic parameters

Inverse micelles

ABSTRACT

Nickel–aluminum layered double hydroxides have been prepared by conventional coprecipitation and by coprecipitation in the presence of a surfactant. The solids have been characterised by several physicochemical techniques. Calcination leads to formation of homogeneously dispersed mixed oxides, which have been characterised as well. The colour properties (lightness and chromaticity coordinates) of both series of solids (layered precursors and calcined ones) have been measured. It has been found that both the preparation method and the calcination treatment have an important effect on the luminosity (whiteness/darkness) of the solids, although the effect on the precise chromaticity coordinates (green/red and blue/yellow) is less marked.

© 2009 Elsevier Inc. All rights reserved.

1. Introduction

Layered double hydroxides (LDHs) constitute a family of layered materials which can be described as brucite layers where a partial Mg^{2+}/M^{3+} substitution has taken place. The positive charge resulting from this substitution is balanced by hydrated counteranions between the layers. The best known example is the mineral hydroxalite, $Mg_6Al_2(OH)_{16}(CO_3)4H_2O$, and numerous compounds with this structure have been prepared with a wide variety of cations in the layers and of interlayer anions [1–5]. These materials have been widely applied as catalysts and catalyst precursors [1,2,6–9], drugs carriers [1,10–14], adsorbents [15], anion scavengers [16–19], composites [20–22], etc., some of these properties arising from their anion exchange ability and from the so-called memory effect, i.e., recovering of the layered structure after being calcined at mild temperatures.

The properties of these compounds are highly dependent on the specific method used to prepare them, usually by coprecipitation, although other methods have been reported [23,24]. In addition, post-preparation treatments (ageing) have been applied usually to improve their crystallinity, and microwave irradiation has proved to be very effective to produce deep changes in several properties [25,26].

Calcination of these compounds leads to a mixture of the corresponding oxides and evolution of the interlayer anion (e.g. as CO_2 from carbonate); if the cations in the original layers are divalent and trivalent ones, and do not undergo any oxidation process during calcination, then the mixture usually contains the corresponding spinel, in addition to the oxide of the divalent

cation (the M^{2+}/M^{3+} ratio in stable LDHs is larger than in stoichiometric spinels). This fact opens new applications for these compounds when one (or both) of the cations is coloured to obtain new ceramic pigments [27,28]. We have previously reported on the preparation and characterisation of different LDHs with transition metal cations in the brucite-like layers, and we have characterised their calcination products, usable as pigments in the ceramic industry [27,29,30]; several colours were developed in these studies, which properties were correlated to the molar fractions of the metal cations and the thermal treatment given. Our current aim is to develop preparation procedures to obtain these ceramic pigments with pre-established morphological properties, as current development in the ceramic industry is based on the use of ink-jet ceramic pigments, needing stable suspensions of the pigments and, as far as possible, a uniform distribution of particles. Consequently, we here report on the preparation of a green pigment from a Ni, Al containing LDH prepared by two alternative routes, namely, conventional coprecipitation and coprecipitation in the presence of a surfactant in order to control aggregation of the elemental particles through formation of inverse micelles and thus controlling the properties of the final product. The solids (both the layered precursors and the calcined ones) have been characterised by several physicochemical techniques and the lightness and chromaticity coordinates have been measured.

2. Experimental

2.1. Sample preparation

All chemicals were from Panreac (PRS quality) and were used without any further purification. Two synthesis routes were used.

* Corresponding author. Fax: +34 923294574.

E-mail address: vrives@usal.es (V. Rives).

In method A, an aqueous solution A1 containing Ni^{2+} and Al^{3+} chlorides (molar ratio 2/1; total cation concentration 2 M) was slowly, dropwise, added into a basic solution A2 (of which volume was twice that of the metal cations solution) at room temperature. Solution A1 had been prepared by dissolving the required amounts of $\text{NiCl}_2 \cdot 6\text{H}_2\text{O}$ and $\text{AlCl}_3 \cdot 6\text{H}_2\text{O}$ in distilled water at room temperature under vigorous stirring; stirring was continued for 40 min and the solution was filtered to remove any solid residue. Solution A2 had been prepared by slow addition of the required amounts of NaHCO_3 and NaOH . The amount of NaHCO_3 was calculated for a molar $\text{Al}^{3+}/\text{CO}_3^{2-}$ ratio equal to 1, while the amount of NaOH was that needed to neutralise HCO_3^- species and to obtain a solid with the hydrotalcite-type structure; the basic solution was left for 45 min to recover room temperature before solution A1 was added.

A greenish precipitate was formed immediately after addition of the first drops of the cations solution. Addition extended along 4 h and the stirring rate was 400 ± 10 rpm (Heidolph RXR-Z051 vertical stirrer). Once addition was complete the suspension was further stirred at room temperature for 20 h; the solid was then filtered in a Büchner funnel (20 cm diameter) with a water vacuum pump. The liquid was colourless with $\text{pH} = 9.8$. The solid was washed four times with portions of 150 mL of distilled water and once more with 500 mL. In each washing step the solid was maintained in contact with water for 30 min before connecting the water vacuum pump. Washing liquids were colourless and pH varied in the 9–9.8 range. After the fifth washing step air was flowed through the cake for 2 h and the solid was spread on a glass plate to dry at room temperature for 4 days, and then it was manually ground in an agate mortar. The solid thus obtained has been named as Ni_2Al_1 .

Method B consisted in addition of the aqueous solution of cations Ni^{2+} and Al^{3+} to a basic solution containing NaOH , NaHCO_3 , iso-octane, butanol and sodium dodecylsulfate (NaDDS), which had been prepared by mixing the aqueous and the organic components previously prepared separately [31]. Under these conditions, the anionic surfactants formed spheroidal reverse micelles in the organic solvent with the hydrophobic chains pointing out into the oil phase. The aqueous phase was prepared by dissolving 6 g (0.072 mol) of NaHCO_3 and 20 g (0.52 mol) of NaOH in 60 mL of bidistilled water. The organic phase was prepared by slow addition of 1.4 g (0.005 mol) of NaDDS to 100 mL of iso-octane also containing 2 mL of butanol. The mixture was vigorously stirred (600 ± 10 rpm) to avoid precipitation of NaDDS in the organic medium.

The compound was prepared at 75°C and the temperature was controlled with a linear temperature heater from Selecta and a model 2MG Statop temperature controller, using a K-type thermocouple. The suspension was also stirred at 600 ± 10 rpm. Once addition of the metal cations solution was started, a greenish solid was formed, which disappeared on stirring, but finally a dense green suspension was formed; the suspension was slowly dropwise added and addition extended along 2 h.

The solid was separated by centrifugation at 3000 rpm for 1 h. The solid showed a gel-like texture, and was washed to remove by-products (mainly NaCl) and unreacted NaDDS. Washing was carried out by heating the solid for 8 h under reflux conditions in a 1:1 water: ethanol mixture (total volume 200 mL) and then the suspension was again centrifuged at 3000 rpm for 1 h. A second washing step was applied, heating the solid under reflux with 100 mL of acetone for 8 h, and then centrifugation at 3000 rpm for 1 h was applied. The whole washing procedure (in water:ethanol and in acetone) was applied once more. The solid finally obtained was dried in open air at room temperature and hand ground in an agate mortar to yield a fine powder. It was stored in a desiccator with anhydrous CaCl_2 . The sample was named as $\text{Ni}_2\text{Al}_1(\text{MI})$.

The solids were calcined in an oven at 1200°C for 1 h at a heating rate of $5^\circ\text{C}/\text{min}$. The calcined solids are named as $\text{Ni}_2\text{Al}_1/1200$ and $\text{Ni}_2\text{Al}_1(\text{MI})/1200$ and showed a mass loss of 38% in both cases with respect to the original solids.

2.2. Characterisation

Element chemical analysis for metals was carried out at Servicio General de Análisis Químico Aplicado (University of Salamanca) by atomic absorption after dissolving the samples in nitric acid, in a Mark-II ELL-240 instrument.

The powder X-ray diffraction (PXRD) patterns were obtained in a Siemens D-500 diffractometer using $\text{CuK}\alpha$ radiation ($\lambda = 1.5450 \text{ \AA}$) connected to a DACO-MP microprocessor using Diffract-AT software. The applied power was 1200 W (40 kV and 30 mA). The scan speed was $2^\circ (2\theta)/\text{min}$, and the crystalline phases were identified using Eva (Graphics Evaluation Program) software, the ASTM files (Joint Committee on Powder Diffraction Standards, JCPDS) and literature data.

Differential thermal analyses (DTA) were recorded in a DTA-7 model instrument from Perkin Elmer, and the thermogravimetric analyses (TG) in a TGA7-HT model thermobalance also from Perkin Elmer, in oxygen flow (30 mL/min). Both instruments were connected to a personal computer through TAC 7/DX interfaces, and the data were analysed using standard software (Pyris, Series Thermal Analysis system, version 3.0) also provided by Perkin Elmer. This software also allowed to determine the derivative TG curves (DTG). The heating rate was $10^\circ\text{C}/\text{min}$ in both cases and the final temperature reached was 830°C (TG) and 1280°C (DTA).

Temperature-programmed reduction (TPR) studies were carried out in a TPR/TPD 2900 model instrument from Micromeritics, equipped with a W–Au thermal conductivity detector and connected to a Olivetti mod. 300-28 acquisition data station. The reducing agent was a 5% (vol) H_2/Ar mixture from L'Air Liquide, circulated through the sample at a flow of 60 mL/min; a heating rate of $10^\circ\text{C}/\text{min}$ and a sample mass of 50 mg were used, in order to optimize the analysis [32]. The amount of hydrogen consumed was determined upon integration of the areas of the peaks, after calibrating the instrument with CuO (from Merck).

The FT-IR spectra were recorded in a M-1700 2B model spectrometer from Perkin Elmer, using Spectrum V.200 software, in the $4000\text{--}400 \text{ cm}^{-1}$ range. The samples were prepared in KBr discs (ca. 1 mg sample/300 mg KBr). Fifty scans were recorded at a nominal resolution of 4 cm^{-1} to improve the signal-to-noise ratio.

The nitrogen adsorption–desorption isotherms of nitrogen at -196°C were recorded in an automatic volumetric instrument from Micromeritics (model ASAP 2000). A portion of 200 mg of sample was used, which was degassed in two steps: first at room temperature for 2–3 h, after which the temperature was raised in 10°C steps (maintained for 10–15 min) up to 110°C at a residual pressure of 10^{-5} mmHg .

Porosity measurements were carried out in a model Poresizer 9320 mercury porosimeter also from Micromeritics. A portion of 0.2–0.25 g of sample was used, degassed at room temperature by applying the following protocol: vacuum was slowly applied up to a residual pressure of ca. 50 mmHg was reached, and was kept for 30 min; then the pressure was lowered to 0.25 mmHg and finally below 0.05 mmHg, which was maintained for 4–6 h. For the mercury intrusion measurements, the pressure was controlled by two different systems: a low pressure one (from ca. 50 to 1500 mmHg) using synthetic air as pressure transducer, and a high pressure one using oil, up to 2200 atm.

Colour of the samples was quantified by using a Konica Minolta colorimeter (Chroma Meter CR 400 model), equipped with a pulsed Xenon lamp. The data were collected by a personal

computer through a RS-232 interface, and were analysed with Color Data CM-100 W Spectra Magic NX software. We used the $L^*a^*b^*$ system (also known as CIELAB) as the colour space, where L^* stands for lightness (ranging from $L^* = 0$ for black to $L^* = 100$ for white), and a^* and b^* are chromaticity coordinates, where negative values for a^* indicate green and positive values indicate red, while negative values for b^* indicate blue and positive values indicate yellow. Three measurements (with three twinkles each) on three different spots were taken for each sample, averaging the results. Samples were placed between flat colourless glasses on a black sample holder. The instrument had been previously calibrated with Minolta white reference CR-A 43 (XYZ parameters 0.3133, 93.80, and 0.3194, respectively).

3. Results and discussion

3.1. Element chemical analysis

Element chemical analysis results for Ni and Al for both compounds are given in Table 1; the Ni/Al molar ratios are also given. The amount of sodium was below the detection level, and only an almost negligible amount of sulphur (0.02% weight) was found for sample $\text{Ni}_2\text{Al}_1(\text{MI})$. The Ni/Al molar ratios were similar in both cases, although ca. 10% larger for sample $\text{Ni}_2\text{Al}_1(\text{MI})$, indicating a lower positive formal charge of the layers in this last case.

3.2. Powder X-ray diffraction

The PXRD patterns for both samples are included in Fig. 1. The overall shape of these patterns corresponds to the expected nature of the crystalline LDHs with the hydroxalcalite-type structure, to which all the signals recorded could be attributed [33]. The maxima were recorded in almost coincident positions for both samples. In both cases the signals recorded at low diffraction angles, due to diffraction by basal planes, are symmetric and rather sharp, while in the medium range of the diagram the signals are broader and asymmetric. This is due to turbostratic disorder in layers stacking, and these peaks are due to diffraction by non-basal planes.

The peaks are sharper and more intense in the diagram of sample $\text{Ni}_2\text{Al}_1(\text{MI})$, for which the doublet close to 2θ 60–65°, due

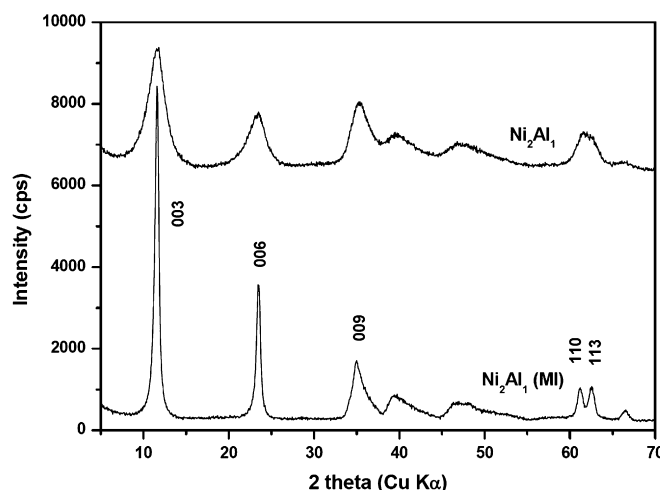


Fig. 1. Powder X-ray diffraction patterns of samples Ni_2Al_1 and $\text{Ni}_2\text{Al}_1(\text{MI})$.

to diffraction by planes (110) and (113), is well resolved and even a new peak at higher diffraction angle is perfectly defined. The larger sharpness of the diffraction maxima for sample $\text{Ni}_2\text{Al}_1(\text{MI})$ can be roughly attributed to a larger crystallinity (larger crystallite size) of this sample.

Lattice parameter c has been calculated from the position of the first diffraction maximum at low diffraction angles. Assuming a 3R packing of the layers, this maximum is due to diffraction by planes (003), and its spacing corresponds to one third of lattice parameter c . To diminish uncertainty (specially for sample Ni_2Al_1 , with broader diffraction maxima), however, the value of c has been averaged from the values determined from spacings measured for planes (003) and (006). This spacing depends on the width of the brucite-like layers, 4.8 Å [34], interlayer hydration, size of the interlayer anion and, for non-spherical anions, its orientation within the interlayer space. Lattice parameter a has been determined from the spacing for the diffraction maximum due to planes (110), recorded at ca. $2\theta = 62^\circ$, $a = 2d(110)$ [2,35–37]. From these lattice parameters and assuming a hexagonal cell, all diffraction maxima have been indexed, as shown in Fig. 1 [38].

Lattice parameters c and a (included in Table 1) are similar to the values reported in the literature for LDHs containing other divalent cations and Al^{3+} in the brucite-like layers and with interlayer carbonate anions [39]. The values for parameter c are coincident within experimental error, and the slight difference in the values for parameter a can be rationalised on the basis of the ionic radii of the layer cations; this parameter is related to the average cation–cation distance in the layer, which depends on their ionic radii. In an octahedral coordination the ionic radius of Ni^{2+} is 0.83 Å, while for Al^{3+} it is 0.675 Å [40]; the larger Ni^{2+} content (larger Ni/Al molar ratio) for sample $\text{Ni}_2\text{Al}_1(\text{MI})$ would account for the larger value of lattice parameter a for this sample. The crystallite sizes, calculated by applying the Scherrer formula [41,42] to diffractions due to planes (003) and (006), are also included in Table 1. As expected from the sharper peaks for sample $\text{Ni}_2\text{Al}_1(\text{MI})$, the crystallite size (measured in the direction perpendicular to the layers) is 4.5 times larger in this sample than for sample Ni_2Al_1 . From these values and taking 7.6 Å as the thickness of a brucite-like layer and an interlayer (actually, the spacing for diffraction due to planes (003), one third of parameter c), we can conclude that the average crystallite is formed by stacking ca. 6 layers in sample Ni_2Al_1 , and 24 layers for sample $\text{Ni}_2\text{Al}_1(\text{MI})$.

Table 1

Element chemical analysis (weight percentage), lattice parameters a and c (Å), crystallite size D (Å), TG data (%), molecular formula, TPR results and specific surface area (mercury intrusion, S_{Hg} , and nitrogen adsorption, S_{BET}) for the layered precursors.

Parameter/sample	Ni_2Al_1	$\text{Ni}_2\text{Al}_1(\text{MI})$
Ni	31.9	35.4
Al	7.8	7.1
$\text{Ni}^{\text{II}}/\text{Al}^{\text{III}}$ molar ratio (solid)	1.90	2.10
a	3.01	3.03
c	22.91	22.87
D	41	179
Mass loss 70–290 °C	12.6	13.4
Mass loss 290–830 °C	23.5	22.1
Mass loss 70–830 °C	36.1	36.5
Molecular formula	$[\text{Ni}_{0.65}\text{Al}_{0.35}(\text{OH})_2](\text{CO}_3)_{0.173}$	$[\text{Ni}_{0.68}\text{Al}_{0.32}(\text{OH})_2](\text{CO}_3)_{0.16}$
Water content per formula	0.74	0.71
TPR $[\text{H}_2]_{\text{exp}}/[\text{H}_2]_{\text{theo}}$	1.09	0.96
S_{Hg} (m^2/g)	13	107
S_{BET} (m^2/g)	<10	119

3.3. Thermal decomposition and solids formed thereof

As one of the aims of this study is the preparation of mixed oxides through thermal decomposition of these LDHs, we have studied their thermal decomposition up to ca. 830 °C under dynamic oxygen or nitrogen atmospheres. No significant differences were found between the results obtained under both atmospheres, and so only the results obtained in oxygen will be shown. The results from the TG analysis (mass loss percentages in the three temperature ranges corresponding to the different decomposition steps) are summarised in Table 1. The TG curves for both samples are shown in Fig. 2. As the decomposition steps are somewhat overlapped, the DTG curves (also shown in this figure) permit an easier comparison of the processes for both samples.

Decomposition of sample Ni₂Al₁ takes place in two well defined steps. According to data in the literature [43,44], the first one should be due to removal of water weakly adsorbed (physisorbed) on the external surface of the crystallites; a small mass loss is observed up to 140–150 °C; such a process seems to be enhanced at 275–290 °C, corresponding to removal of water molecules from the interlayer, where it was bonded via hydrogen bonds to layer hydroxyl groups and interlayer carbonate anions [33]. Unfortunately the gases evolved during thermal decomposition could not be analysed. Such a two steps process for water removal can be easily identified in the DTG curve, with two minima roughly corresponding with the two sections of the TG curve showing slightly different slopes. The second decomposition step, identified by the DTG minimum at ca. 400 °C, corresponds to decomposition of the layers, i.e., water removal through condensation of layer hydroxyl groups, and CO₂ release from interlayer carbonate anions. After this second effect no major mass loss takes place even up to 830 °C, and only a continuous,

almost negligible mass loss is observed. This has been attributed [45] to removal of carbon dioxide from residual carbonate species.

The DTA curve (inset in Fig. 2) also shows two minima, corresponding to two endothermic processes. The first minimum is very broad, and should correspond to the two first mass losses (physisorbed and interlayer water removal), while the second one, with a rather sharp shape, should be associated to the dehydroxylation and decarbonation processes.

Decomposition of sample Ni₂Al₁(MI) follows a similar pattern at medium and high temperatures, although some differences are evident in the low temperature region. So, the DTG curve clearly shows a weak minimum below 110 °C which could be tentatively attributed to removal of traces of acetone (boiling point 56 °C) and/or isooctane (b.p. 99 °C) which could remain physisorbed on the external surface of the crystallites. The mass loss responsible for the DTG minimum below 300 °C should be due to removal of interlayer water molecules, while the last loss (DTA minimum at ca. 400 °C, same position as for sample Ni₂Al₁) should be due to dehydroxylation and decarbonation processes. Similar comments as for sample Ni₂Al₁ can be applied to the DTA curve (inset in Fig. 2). It should be noticed, however, that dehydration takes place at a higher temperature for sample Ni₂Al₁(MI) than for sample Ni₂Al₁, probably because of the larger crystallinity of the former, which would permit to establish more and stronger hydrogen bonds between water molecules and layer hydroxyl groups and interlayer carbonate anions.

The crystalline phases in the solid residue formed at 830 °C (TG) or 1280 °C (DTA) were determined by PXRD, Fig. 3. The pattern for the 830 °C residue of sample Ni₂Al₁(MI) shows only three rather weak diffraction maxima which positions coincide with those for the rock salt structure of nickel oxide (JCPDS file 22-1189). For the DTA residue (1280 °C) of the same sample the crystallinity of this oxide is enhanced, while other diffraction

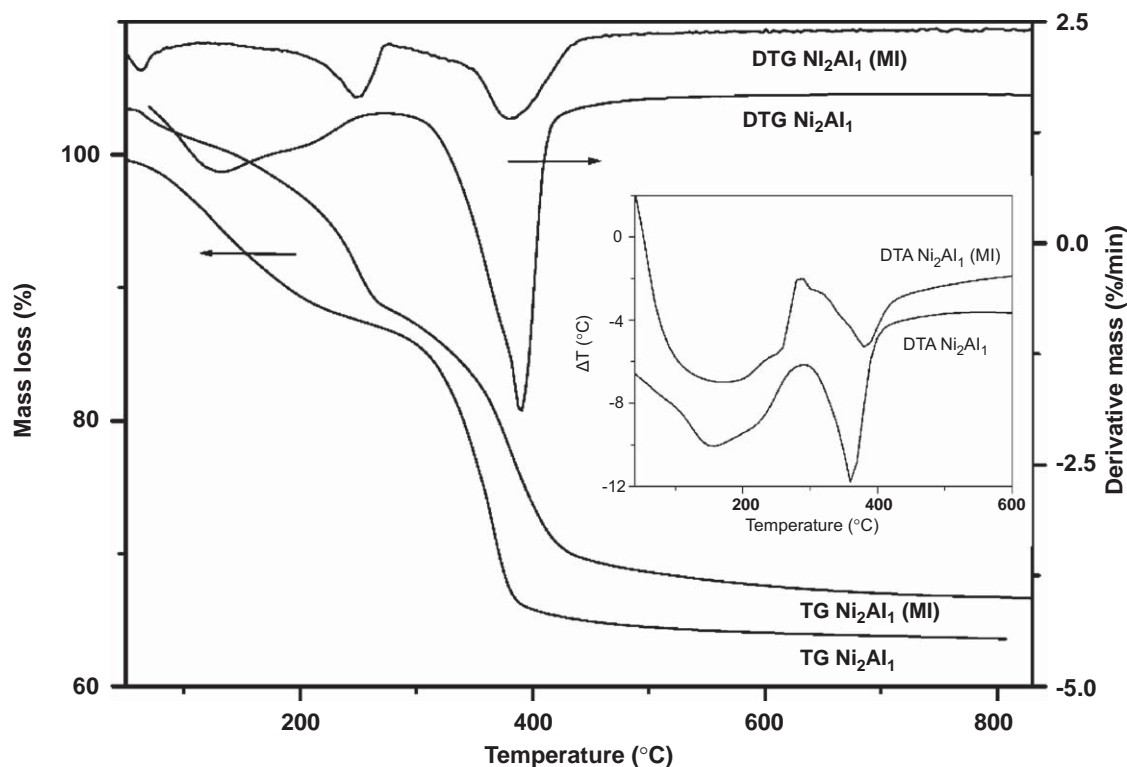


Fig. 2. Thermogravimetric (bottom, left y-axis) and differential thermogravimetric (top, right y-axis) diagrams of the samples. Inset: differential thermal analysis curves. All analysis performed in oxygen.

maxima develop. Two maxima coinciding with those of NiO and the new ones correspond to the spinel structure, NiAl_2O_4 (JCPDS file 10-0339). It is not clear, however, where the Al^{3+} cations were located in the residue formed at 830 °C, well dissolved in the NiO structure, or forming an amorphous phase, undetectable by PXRD. In the former case the signals due to NiO would have been recorded at larger diffraction angles (because of the smaller ionic radius of Al^{3+} with respect to Ni^{2+}); however, the relative broadness of the diffraction signals for the sample calcined at 830 °C does not permit locating the maxima with enough accuracy to conclude formation (or not) of the solid solution.

A similar behaviour is observed for sample Ni_2Al_1 , with broad peaks when calcined at 830 °C, sharpening when the calcination temperature was raised to 1280 °C. However, in this case some extremely weak maxima due to the NiAl_2O_4 spinel phase are already observed for the sample calcined at 830 °C, and the overall sharpness of the maxima recorded for the sample calcined at 1280 °C (and so the crystallinity of the sample) is larger than for the calcined sample $\text{Ni}_2\text{Al}_1(\text{MI})$.

We should then conclude that calcination of these two samples at 830 °C leads to formation of a solid with the rock salt structure of NiO, where Al^{3+} cations could be dissolved forming a solid solution, or forming an amorphous aluminum oxide phase (although the presence of an amorphous phase in a solid calcined at 830 °C should be hardly expected). Calcination at 1280 °C leads to formation of the NiAl_2O_4 spinel, in addition to NiO. The NiAl_2O_4 spinel has [46] a partially inverse structure with $\lambda = 0.38$, a value very close to that ($\lambda = 0.33$) corresponding to a random distribution of the cations in octahedral and tetrahedral holes.

The molecular formula of the samples, as determined from element chemical analysis (to determine the composition of the hydroxalcite-type layers) and assuming carbonate as the only interlayer anion, and from the TG results (to determine the interlayer water content) are also included in Table 1. The maximum amount of interlayer water content can be calculated assuming a close packing of the interlayer by water molecules and carbonate anions [47]; the values are 1.48 and 1.52 water molecules per molecular formula for samples Ni_2Al_1 and $\text{Ni}_2\text{Al}_1(\text{MI})$, respectively. The experimental values are ca. 50% of the maximum ones, indicating that a more open structure is adopted, probably to facilitate hydrogen bonding between the water molecules and the layer hydroxyl groups and the interlayer carbonate anions.

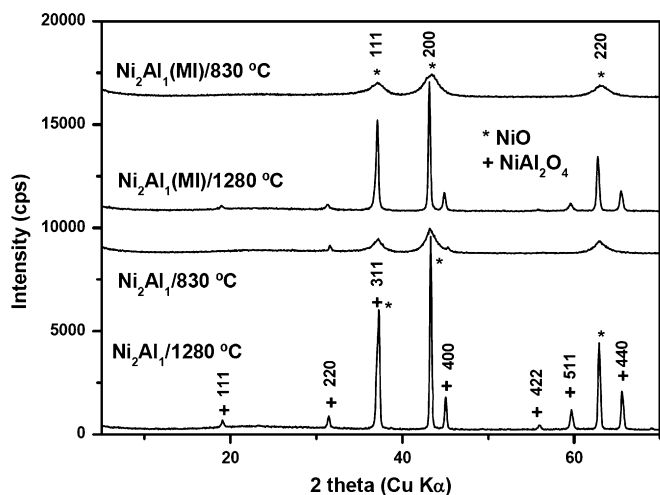


Fig. 3. Powder X-ray diffraction patterns of the residues of the TG (830 °C) and DTA (1280 °C) analyses.

3.4. Temperature-programmed reduction

The TPR curves for both samples are shown in Fig. 4. It should be recalled that decomposition along the TPR experiments takes place in a reducing atmosphere, while the TG and DTA analyses were carried out in oxygen, so the processes taking place along both sets of experiments should not necessarily occur at coincident temperatures.

According to the literature [43,48], under the experimental conditions here used carbonate is removed as CO_2 before being reduced to coke or methane [49] and Al^{3+} cations are not reduced, while Ni^{2+} is quantitatively reduced to the zero-valent state [50]. Hydrogen consumption stoichiometrically corresponds to one hydrogen molecule per Ni^{2+} cation in the solid.

Upward deviation of the curve means hydrogen consumption (i.e., lower hydrogen concentration in the gas exiting from the sample chamber than flowing through the reference branch of the TPR instrument), while a downwards deviation would eventually stand for hydrogen enrichment by hydrogen released from the sample. The curves have been normalised by referring them per unit mass of nickel in the samples. The curve for sample Ni_2Al_1 ,

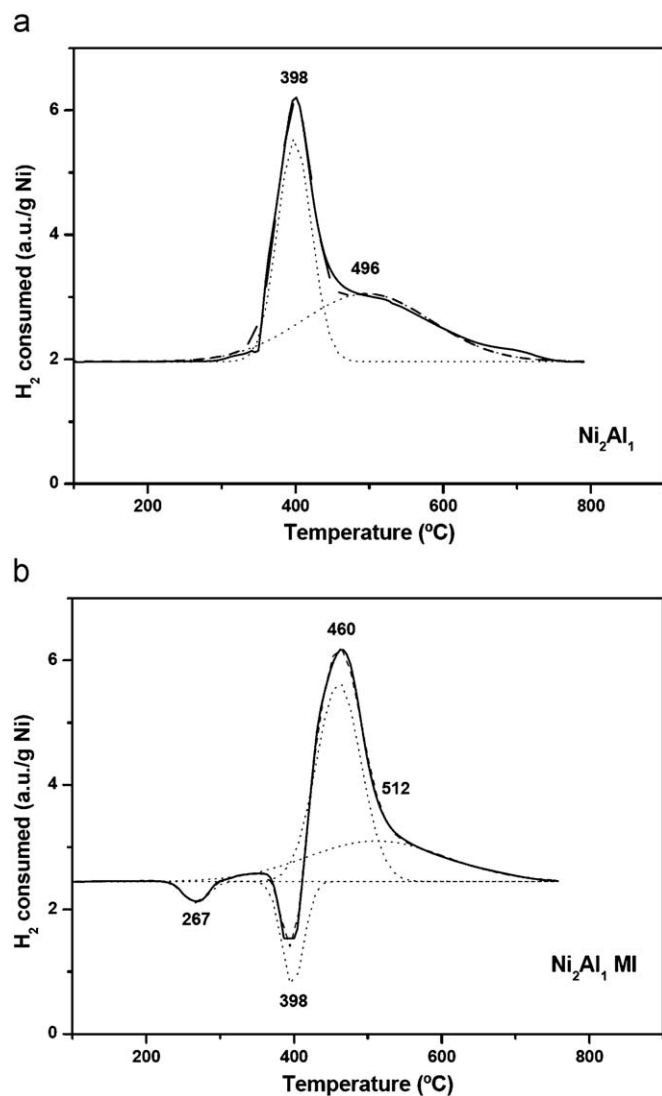


Fig. 4. Temperature-programmed reduction curves for sample Ni_2Al_1 (a) and $\text{Ni}_2\text{Al}_1(\text{MI})$ (b). The deconvolution curves and the calculated curve are also shown. (Dotted line: component curves; solid line: experimental data; dashed line: sum of component lines).

Fig. 4(A), shows a maximum at 398 °C with a shoulder at 496 °C. However, for sample $\text{Ni}_2\text{Al}_1(\text{MI})$, two weaker minima are recorded at 267 and 398 °C in addition to a maximum at 460 °C and a shoulder close to 515 °C. The origin of the minima remains uncertain, although they can be tentatively attributed to release of hydrogen from decomposition of physisorbed acetone or iso-octane residues, a process also detected in the thermal analysis studies (Fig. 2); the presence of these species can be also concluded from the FT-IR spectrum of this sample (see below). These two hydrogen release processes will not be further considered.

A Gaussian-type model was applied for an approximate deconvolution of the TPR curves. Two components were found in both cases. The maxima are recorded at 398 and 496 °C for sample Ni_2Al_1 , and their relative intensities (by integrating the area under the curve) are 45:55. Regarding sample $\text{Ni}_2\text{Al}_1(\text{MI})$, also two components were obtained, with maxima at 460 and 512 °C (i.e., 60 °C higher than for sample Ni_2Al_1), with relative intensities 60:40. The shift in the positions of the maxima may have a kinetics origin, due to the restricted flow of hydrogen (or water vapour formed upon Ni^{2+} reduction) in the larger crystallites of sample $\text{Ni}_2\text{Al}_1(\text{MI})$ than in the more “amorphous” sample Ni_2Al_1 . However, it should be recalled that only Ni^{2+} cations are able to be reduced along these experiments. It should be also noticed that while the first process takes place in a rather narrow temperature range (the width of the maximum at half height is 45 °C), it results much broader (width at half height 180 °C) for the second one. The presence of two reduction processes probably suggests that in both samples there are two structurally different Ni^{2+} species. In the original LDH structure the metal cations are located in octahedral holes of the brucite-like layers, but the sample is decomposed (and structurally modified) along the TPR experiments, and so it would be hardly accepted that at 400 °C under a reducing atmosphere all Ni^{2+} species are still in octahedral holes. On the other hand, formation of the NiO and NiAl_2O_4 spinel phases (which presence was concluded from PXRD analysis of the residues formed after calcination above 1000 °C) cannot be discarded (or accepted) during the TPR analysis, despite the heating conditions (atmosphere surrounding the sample) were absolutely different. Although further insight in the actual nature of the species being reduced would be desirable, we can tentatively ascribe this behaviour well to the reduction of Ni^{2+} cations existing in the borders of the crystallites or further inside them, or to reduction of Ni^{2+} cations existing in two structurally different environments, octahedral and tetrahedral holes. Moreover, the relative concentration of the low temperature reducible species is larger for sample $\text{Ni}_2\text{Al}_1(\text{MI})$ than for sample Ni_2Al_1 .

If the total hydrogen consumption is calculated, the Ni/H_2 molar ratio corresponds to 1.09 and 0.96, respectively, for samples Ni_2Al_1 and $\text{Ni}_2\text{Al}_1(\text{MI})$. These values are acceptably close to the stoichiometric one (1.00), taking into account the accuracy usually accepted for this technique.

3.5. FT-IR spectroscopy

The FT-IR spectra of these two samples are shown in Fig. 5. They are typical of the LDH structure with interlayer carbonate anions. The noticeable larger sharpness of the low wavenumber bands for sample $\text{Ni}_2\text{Al}_1(\text{MI})$ should be related to the larger crystallinity of this sample, but the bands are roughly recorded in the same positions in the spectra of both samples. The broad band at 3500–3450 cm^{-1} is due to the O–H stretching modes of layer hydroxyl groups and water molecules. The broadness arises from the very different strengths of hydrogen bonding between these species. The band is asymmetric and a broad shoulder around

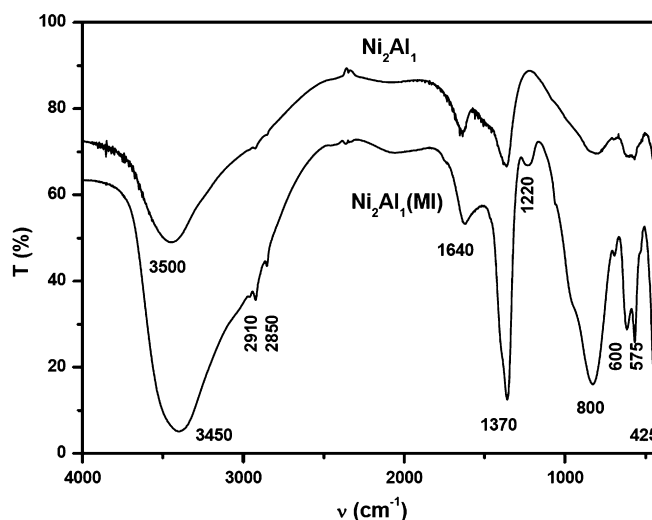


Fig. 5. FT-IR spectra of samples Ni_2Al_1 and $\text{Ni}_2\text{Al}_1(\text{MI})$.

3000 cm^{-1} is due to the O–H stretching mode of interlayer water molecules hydrogen-bonded to interlayer carbonate anions. Water molecules are also responsible for the medium-weak band at 1640 cm^{-1} , due to their angular deformation mode [33]. The negative doublet around 2200 cm^{-1} is due to a miscancelation of the mode due to atmospheric CO_2 .

The band at 1370 cm^{-1} is due to the antisymmetric ν_3 mode of carbonate anions; the shoulder close to 1470 cm^{-1} is due to the decreased symmetry of this anion from D_{3h} to C_{3v} (or even C_{2v}) upon hydrogen bonding with other species (water molecules and hydroxyl groups from the brucite-type layers) in the interlayer. This decreased symmetry is also responsible for IR-activation of the ν_1 mode, recorded as a weak shoulder at 1040 cm^{-1} [33,51,52].

The extremely weak bands just below 3000 cm^{-1} are due to the C–H stretching modes of organic species existing in the laboratory atmosphere. However, in the spectrum of sample $\text{Ni}_2\text{Al}_1(\text{MI})$ they are markedly stronger than in the spectrum of sample Ni_2Al_1 . Moreover, the spectrum of the former sample shows a band, absent in the spectrum of the latter, at 1220 cm^{-1} which can be ascribed to the antisymmetric S–O stretching mode of sulphate species, in agreement with the low sulphur content (0.02%) in this sample.

The bands at 600, 570 and 425 cm^{-1} are due to Ni–O–Al deformation mode and Ni–O and Al–O stretching modes [33] and, as the other bands, are much better defined in the spectrum of sample $\text{Ni}_2\text{Al}_1(\text{MI})$ than in that for sample Ni_2Al_1 .

3.6. Surface area and porosity

Results from surface area and porosity analysis, both through nitrogen adsorption and mercury intrusion (inset), for sample $\text{Ni}_2\text{Al}_1(\text{MI})$, are shown in Fig. 6. The nitrogen adsorption capacity of sample Ni_2Al_1 was very low. The nitrogen adsorption curve corresponds to type IV in the IUPAC classification [53] with a narrow type H3 hysteresis loop [54], suggesting a mesoporous, uniform structure of the pores. It should be noticed that the height of the interlayer (populated by carbonate anions and water molecules) does not permit inclusion of nitrogen molecules and consequently the interlayer space (actually corresponding to micropores) is not measured by this technique. The specific surface area values, measured by the BET method from the nitrogen adsorption isotherms, were 119 and less than 10 m^2/g for samples $\text{Ni}_2\text{Al}_1(\text{MI})$ and Ni_2Al_1 , respectively. The values calculated from the mercury intrusion experiments were roughly coincident,

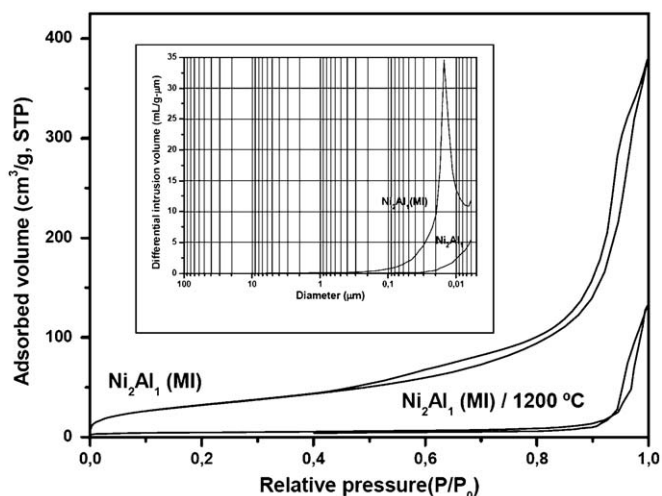


Fig. 6. Nitrogen adsorption–desorption isotherms for uncalcined and calcined $\text{Ni}_2\text{Al}_1(\text{MI})$ sample. Inset: Pore size distribution curve for the uncalcined samples as measured by mercury intrusion.

107 and $13 \text{ m}^2/\text{g}$, respectively. The difference between the values for both samples indicates that the preparation method has an outstanding influence not only on the crystallinity of the particles and ordering of the interlayer species, but also on the texture properties.

The pore size distribution curves, as measured from the mercury intrusion experiments, are also included in Fig. 6; only a sharp maximum (ca. 15 nm) is obtained for sample $\text{Ni}_2\text{Al}_1(\text{MI})$, confirming the ordered pore structure of this sample.

If we are dealing with non porous particles, we would expect that as the size of the crystallites increase, the specific surface area would decrease. However, the results here obtained show just the opposite behaviour, i.e., sample $\text{Ni}_2\text{Al}_1(\text{MI})$, formed by larger, ordered crystallites ($D = 180 \text{ \AA}$) show a larger specific surface area than sample Ni_2Al_1 . The presence of mesopores with a radius close to 15 nm in sample $\text{Ni}_2\text{Al}_1(\text{MI})$ would, however, account for the larger surface area development.

3.7. Characterisation of the calcined solids

The PXRD patterns of the calcined solids are essentially coincident with those reported in Fig. 3 for the DTA residues, with diffraction maxima corresponding to NiO (JCPDS file 22–1189) and NiAl_2O_4 (file 10–0339). The maxima are sharper for the Ni_2Al_1 precursor, indicating slightly larger crystallites in this sample. These PXRD patterns have been indexed for a cubic system and the values for lattice parameters a for both crystalline phases are included in Table 2 [46]. Maxima due to diffraction by planes (200) and (220) were used to determine the parameter for the NiO crystallites, (111) being ignored because of its rather low intensity and coincidence with the most intense diffraction of the spinel phase. Maxima due to diffraction by planes (111), (311), (400), (511), and (440) were used for the spinel phase, all being very sharp and rather intense. The values reported in Table 2 for the spinel phase are very close for both samples and also close to that reported in the literature [55] for the partially inverse ($\lambda = 0.375$) NiAl_2O_4 spinel, 8.046 \AA . Table 2 also includes the average crystallite size of the calcined solids. This parameter markedly increases for NiO formed after calcinations of $\text{Ni}_2\text{Al}_1(\text{MI})$ at $1200 \text{ }^\circ\text{C}$.

The TPR curves for the calcined samples are shown in Fig. 7. The lack of “negative” effects for the calcined $\text{Ni}_2\text{Al}_1(\text{MI})$ sample confirms that those recorded for the uncalcined samples did

Table 2

Lattice parameter a (\AA), crystallite size D (\AA), TPR results and specific surface area (nitrogen adsorption) for the solids calcined at $1200 \text{ }^\circ\text{C}$.

Parameter/sample	$\text{Ni}_2\text{Al}_1/1200$		$\text{Ni}_2\text{Al}_1(\text{MI})/1200$	
	NiO	NiAl_2O_4	NiO	NiAl_2O_4
a	4.189	8.040	4.189	8.061
D	350	330	450	340
TPR $[\text{H}_2]_{\text{exp}}/[\text{H}_2]_{\text{theo}}$	1.08		1.05	
S_{BET} (m^2/g)	<6		16.0	

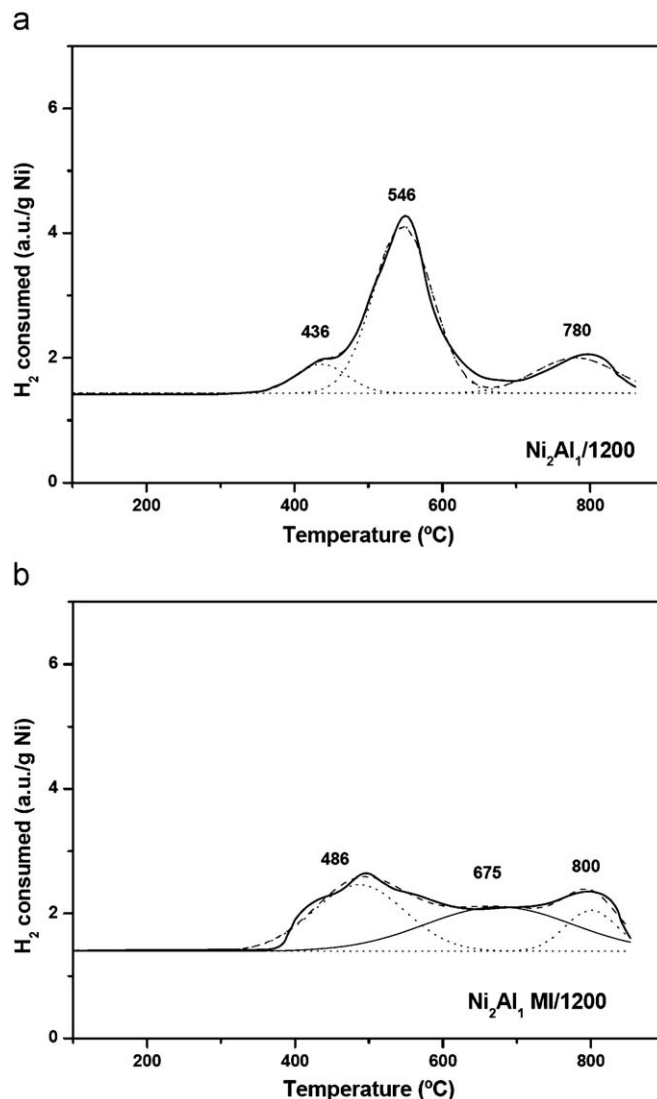


Fig. 7. Temperature-programmed reduction curves for calcined ($1200 \text{ }^\circ\text{C}$) sample Ni_2Al_1 (a) and $\text{Ni}_2\text{Al}_1(\text{MI})$ (b). The deconvolution curves and the calculated curve are also shown. (Dotted line: component curves; solid line: experimental data; dashed line: sum of component lines).

correspond to the organic impurities adsorbed on the crystallites surface. While for the uncalcined solids two maxima could be detected (although the second one appeared as a broad shoulder of the most intense one at lower temperature, Fig. 4), in this case the curves recorded could be deconvoluted into three maxima, at different positions (temperatures) and with different intensities (10:70:20 for sample $\text{Ni}_2\text{Al}_1/1200$, and 40:45:15 for sample $\text{Ni}_2\text{Al}_1(\text{MI})/1200$). Of course, of all them correspond to reduction of Ni^{2+} cations in different structural locations, and in

this case reduction occurs on the well stabilised structures of NiO (rock salt type) and NiAl₂O₄ (spinel). According to the PXRD data above commented, the spinel shows a partially inverse structure, and so Ni²⁺ occupy (probably in an almost random distribution, for which $\lambda = 0.333$) both octahedral and tetrahedral sites, while in NiO only octahedral sites are occupied. Consequently, we might have up to three different structural environments for Ni²⁺ cations: (i) in octahedral sites in the NiO structure, (ii) in octahedral sites in the spinel structure, and (iii) in tetrahedral sites in the spinel structure. Probably, the easiness with which Ni²⁺ species are reduced (in other words, the reduction temperature) depends on their precise structural location, thus accounting for the three reduction components determined.

From these curves it is evident that the preparation procedure has a marked effect on the nature of the calcination products and their reducibility. The maxima are recorded at higher temperatures for the sample prepared in an organic medium. The slight difference in the value of lattice parameter *a* for the spinel phase could be due to a different degree of inversion of the spinel crystallites in both samples, thus changing the population of Ni²⁺ cations in octahedral and tetrahedral sites, with different ionic radii. The ionic radii of tetrahedrally coordinated Ni²⁺ and Al³⁺ are 0.69 and 0.53 Å, while in octahedral coordination these values are 0.83 and 0.68 Å, respectively [56].

The larger the location of Ni²⁺ cations in tetrahedral sites, the larger the inversion degree of the structure and the larger the value of lattice parameter *a*. The third component reduction peak has roughly the same relative intensity in both cases, and then could be tentatively ascribed to reduction of Ni²⁺ in the octahedral holes of the NiO phase. The intensity of the second reduction maximum decreases on passing from sample Ni₂Al₁/1200 to sample Ni₂Al₁(MI)/1200, and could be then tentatively ascribed to reduction of Ni²⁺ cations in octahedral sites of the spinel phase. For both phases the H₂/Ni ratio, Table 2, is equal to the expected value (1.0) within experimental error, indicating total reduction of the Ni²⁺ species in the temperature range studied.

The calcined samples show an extremely low ability for nitrogen adsorption in all the relative pressure range studied. The specific surface areas values determined by the BET method are given in Table 2. Although the specific surface area for sample Ni₂Al₁(MI)/1200 is reduced to ca. 13% of the value for the uncalcined sample, it is still larger than the value measured for the calcined Ni₂Al₁ sample. The isotherm for the former sample, Fig. 6, belongs to type IV in the IUPAC classification with a type H3 hysteresis loop extending in the relative pressure range 0.45–1.0, suggesting the presence of pores only in the mesoporosity range.

3.8. Colour study

Colour coordinate values (*L**, *a** and *b**) for all samples (original and calcined) studied are given in Table 3. The corrected parameters after subtracting the values corresponding to the sample holder used as a reference, and the values for colour difference calculated using the equation

$$\Delta E^* = \sqrt{(\Delta L^*)^2 + (\Delta a^*)^2 + (\Delta b^*)^2}$$

[57,58] are also included in this table.

Luminosity of the solids decreases after calcination (i.e., they become darker). More positive values of Δb^* indicate that calcined samples are more yellowish than the precursor solids. Regarding parameter *a** (red–green), the values measured are always negative, without any evident regular change upon calcination. So, the greener sample leads to a sample with a lesser negative Δa^* value after calcination, while the green colour is enhanced

Table 3

Colour parameters of the samples prepared.

Sample	<i>L</i> *	<i>a</i> *	<i>b</i> *	ΔL^*	Δa^*	Δb^*	$\Delta E_{a^*b^*}$
Ni ₂ Al ₁	56.76	−21.86	−1.1	17.17	−21.61	0.76	27.61
Ni ₂ Al ₁ (MI)	65.96	−14.29	−5.15	26.37	−14.04	3.29	30.05
Ni ₂ Al ₁ /1200	45.13	−9.21	1.28	5.54	−8.96	3.14	10.99
Ni ₂ Al ₁ (MI)/1200	54.56	−17.54	7.47	14.97	−17.29	9.33	24.70

*L** (luminosity), *a** (red > 0 > green), *b** (yellow > 0 > blue).

after calcination, if the original sample had been prepared in an organic medium.

It can be also observed that the preparation procedure has a regular effect on the luminosity of the solids, this parameter showing larger values for samples prepared in an organic medium than for those prepared by conventional precipitation. A similar behaviour is observed for parameter *b** (negative for blue and positive for yellow), the solids prepared in an organic medium showing larger Δb^* values.

Finally, the parameters are closer for the precursor solids and decrease upon calcination, although such a decrease is less marked for samples prepared in an organic medium.

4. Conclusions

Two different routes have been used to prepare Ni,Al LDHs with almost coincident chemical compositions. Larger and more ordered crystals were obtained following the inverse micelles route, probably because within the hydrophilic core of the micelles a slow—and thus better ordered—growing of the crystals may take place. Moreover, if the micelles have a narrow distribution size, a homogeneous distribution of the inorganic particles would exist, thus accounting for the homogeneous interparticle mesopores determined by mercury intrusion.

Thermal decomposition leads to distorted NiO at 830 °C, finally leading to a mixture of NiO and partially inverse NiAl₂O₄ spinel at 1280 °C; the existence of Ni²⁺ cations in three different structural environments is evidenced from the TPR measurements.

Regarding the colour coordinates of these solids, an enhancement of the green colour is observed for the sample prepared in an organic medium upon calcination; this sample also shows a larger luminosity than that prepared by conventional coprecipitation.

Acknowledgments

Authors thank financial support from MEC (grant MAT2006-10800-C02-01) and Junta de Castilla y León (grant SA024A06). The assistance of Mr. A. Montero to obtain some of the experimental results is also acknowledged.

References

- [1] V. Rives (Ed.), Layered Double Hydroxides: Present and Future, Nova Science Publishers, Inc., New York, 2001.
- [2] F. Cavani, F. Trifiró, A. Vaccari, Catal. Today 11 (1991) 173.
- [3] X. Duan, D.G. Evans (Eds.), Layered double hydroxides, Struct. Bonding 119 (2005).
- [4] F. Wypych, K.G. Satyanarayana (Eds.), Clay Surfaces: Fundamentals and Applications, Elsevier, Amsterdam, 2004.
- [5] V. Rives, M.A. Ulibarri, Coord. Chem. Rev. 181 (1999) 61.
- [6] A. Vaccari, Catal. Today 41 (1998) 53.
- [7] D. Carriazo, C. Martín, V. Rives, Eur. J. Inorg. Chem. (2006) 4608.
- [8] G. Centi, S. Perathoner, Microp. Mesopor. Mater. 170 (2008) 3.
- [9] S. Albertazi, F. Basile, A. Vaccari, Catalytic properties of hydrotalcite-type anionic clays, in: F. Wypych, K.G. Satyanarayana (Eds.), Clay Surfaces: Fundamentals and Applications, Elsevier, Amsterdam, 2004 (Chapter 17).

- [10] J.H. Yang, Y.S. Han, M. Park, T. Park, S.J. Hwang, J.H. Choy, *Chem. Mater.* 19 (2007) 2679.
- [11] M. del Arco, E. Cebadera, S. Gutiérrez, C. Martín, M.J. Montero, V. Rives, J. Rocha, M.A. Sevilla, *J. Pharm. Sci.* 93 (2004) 1649.
- [12] J.H. Yang, S.Y. Lee, Y.S. Han, K.C. Park, J.H. Choy, *Bull. Korean Chem. Soc.* 24 (2003) 499.
- [13] L. Peroli, V. Ambrogio, B. Bertini, M. Ricci, M. Nochetti, L. Latterini, C. Rossi, *Eur. J. Pharm. Biopharm.* 62 (2006) 185.
- [14] S.J. Choy, J.M. Oh, T. Park, J.H. Choy, *J. Nanosci. Nanotech.* 7 (2007) 4017.
- [15] N.N. Das, J. Konar, M.K. Mohanta, S.C. Srivastava, *J. Colloid Interface Sci.* 270 (2004) 1.
- [16] F. Kovanda, E. Kovacsova, D. Koloušek, *Collect. Czech. Chem. Commun.* 64 (1999) 1517.
- [17] N.K. Lazaridis, T.A. Pandi, K.A. Matis, *Ind. Eng. Chem. Res.* 43 (2004) 2209.
- [18] E. Álvarez-Ayuso, H.W. Nugteren, *Water Res.* 39 (2005) 2535.
- [19] C. Barriga, M. Gaitán, I. Pavlovic, M.A. Ulibarri, M.C. Hermosín, J. Cornejo, *J. Mater. Chem.* 12 (2002) 1027.
- [20] F. Leroux, J.-P. Besse, Layered double hydroxide/polymer nanocomposites, in: F. Wypych, K.G. Satyanarayana (Eds.), *Clay Surfaces: Fundamentals and Applications*, Elsevier, Amsterdam, 2004 (Chapter 16).
- [21] X. Wang, Q. Zhang, *Polym. Int.* 53 (2004) 698.
- [22] R. Kaluskova, M. Novota, Z. Vymazal, *Polym. Degrad. Stabl.* 85 (2004) 903.
- [23] A. Roy, C. Forano, J.P. Besse, Layered double hydroxides: synthesis and post-synthesis modifications, in: V. Rives (Ed.), *Layered Double Hydroxides: Present and Future*, Nova Science Publishers, Inc., New York, 2001 (Chapter 1).
- [24] J. He, M. Wei, B. Li, Y. Kang, D.G. Evans, X. Duan, Preparation of layered double hydroxides in: X. Duan, D.G. Evans, (Eds.), *Layered Double Hydroxides, Structure and Bonding*, vol. 119, (2005) pp. 89–119.
- [25] P. Benito, I. Guinea, M. Herrero, F.M. Labajos, V. Rives, *Z. Anorg. Allg. Chem.* 633 (2007) 1815.
- [26] M. Herrero, P. Benito, F.M. Labajos, V. Rives, *Catal. Today* 128 (2007) 129.
- [27] J.M. García-García, M.E. Pérez-Bernal, R.J. Ruano-Casero, V. Rives, *Solid State Sci.* 9 (2007) 1115.
- [28] I. Nebot-Díaz, M. Marchal, M. Irún, J.B. Carda, *Nuevas tecnologías para el sector cerámico/New Technologies for Ceramic Industry*, Universitat Jaume I, Castelló, 2000.
- [29] M.E. Pérez-Bernal, R.J. Ruano-Casero, V. Rives, *Ceramics Silikaty* 48 (2004) 145.
- [30] R.J. Ruano-Casero, M.E. Pérez-Bernal, V. Rives, *Z. Anorg. Allg. Chem.* 631 (2005) 2142.
- [31] G. Hu, N. Wang, D. O'Hare, J. Davis, *J. Mater. Chem.* 17 (2007) 2257.
- [32] P. Malet, A. Caballero, *J. Chem. Soc. Faraday Trans. I* 84 (1988) 2369.
- [33] S. Kannan, A. Narayanan, C.S. Swamy, *J. Mater. Sci.* 31 (1996) 2353.
- [34] M.A. Drezdon, *Inorg. Chem.* 27 (1988) 4628.
- [35] A.S. Bookin, V.I. Cherkashin, V.A. Drits, *Clays Clay Miner.* 41 (1993) 558.
- [36] M.A. Ulibarri, F.M. Labajos, V. Rives, R. Trujillano, W. Kagunya, W. Jones, *Inorg. Chem.* 33 (1994) 2592.
- [37] M.A. Ulibarri, F.M. Labajos, V. Rives, R. Trujillano, W. Kagunya, W. Jones, *Mol. Cryst. Liq. Cryst.* 167 (1994) 244.
- [38] P. Gay, *The Crystalline State. An Introduction*, third ed, Oliver & Boyd, Edinburgh, 1972.
- [39] V.A. Drits, A.S. Bookin, *Crystal structure and X-ray identification of layered double hydroxides*, in: V. Rives (Ed.), *Layered Double Hydroxides: Present and Future*, Nova Science Publishers, Inc., New York, 2001 (Chapter 2).
- [40] W.W. Porterfield, *Inorganic Chemistry. A Unified Approach*, second ed, Academic Press Inc., London, 1993, p. 82.
- [41] H.P. Klug, L.E. Alexander, *X-ray Diffraction Procedures*, John Wiley and Sons, Inc., New York, 1974.
- [42] R. Jenkins, J.L. De Vries, in: *Worked examples of X-ray Analysis*, second ed., Phillips Technical Library, Macmillan Press Ltd., London, 1978.
- [43] V. Rives, Study of layered double hydroxides by thermal methods, in: V. Rives (Ed.), *Layered Double Hydroxides: Present and Future*, Nova Science Publisher, Inc., New York, 2001 (Chapter 4).
- [44] Ts. Stanimirova, I. Vergilov, G. Kirov, N. Petrova, *J. Mater. Sci.* 34 (1999) 4153.
- [45] T. Hibino, Y. Yamashita, K. Kosuge, A. Tsunashima, *Clays Clay Miner.* 43 (1995) 427.
- [46] A.W. Wells, *Química Inorgánica Estructural*, Editorial Reverté, Barcelona, 1978.
- [47] S.K. Yun, T.J. Pinnavaia, *Chem. Mater.* 7 (1995) 348.
- [48] V. Rives, M.A. Ulibarri, A. Montero, *Appl. Clay Sci.* 10 (1995) 83.
- [49] V. Rives, O. Prieto, A. Dubey, S. Kannan, *J. Catal.* 220 (2003) 161.
- [50] M. Jitianu, M. Balasoiu, R. Marchidan, M. Zaharescu, D. Crisan, M. Craiu, *Int. J. Inorg. Mater.* 2 (2000) 287.
- [51] F.M. Labajos, V. Rives, *Inorg. Chem.* 35 (1986) 5313.
- [52] J.T. Klopogge, R.L. Frost, Infrared and Raman spectroscopic studies of layered double hydroxides (LDHs), in: V. Rives (Ed.), *Layered Double Hydroxides: Present and Future*, Nova Science Publisher, Inc., New York, 2001 (Chapter 5).
- [53] A.R. Paniago, *An. Quim.* 85 (1986) 386.
- [54] K.S.W. Sing, D.H. Everett, R.A.W. Haul, L. Moscou, R. Pierotti, J. Rouquerol, T. Siemieniowska, *Pure Appl. Chem.* 57 (1985) 603.
- [55] C.N.R. Rao, J. Gopalakrishnan, *New Directions in Solid State Chemistry*, second ed, Cambridge University Press, Cambridge, 1997.
- [56] J.E. Huheey, E.A. Keiter, R.L. Keiter, *Inorganic Chemistry. Principles of Structure and Reactivity*, fourth ed, Harper Collins College Publishers, New York, 1993, p. 114.
- [57] P. Escribano López, J.B. Carda Castelló, E. Cordoncillo Cordoncillo, *Enciclopedia Cerámica, Tomo I: Esmaltes y pigmentos cerámicos*, Universidad Jaime I, Castellón, 2001.
- [58] <<http://www.konicaminolta.com/instruments/knowledge/index.html>>.